Peer-reviewed version available at Crystals 2018, 8, 71; doi:10.3390/cryst8020071

Brief review of the effects of pressure on wolframite-type oxides

D. Errandonea[1] and J. Ruiz-Fuertes[1,2]

[1]*Departament de Física Aplicada-ICMUV, MALTA Team, Universitat de València, 46100 Burjassot, Spain*

[2]*Departamento de Ciencias de la Tierra y Física de la Materia Condensada, MALTA Team, Universidad de Cantabria, 39005 Santander, Spain*

In this article we review the advances that have been made on the understanding of the high-pressure structural, vibrational, and electronic properties of wolframite-type oxides since the first works in the early 1990s. Mainly tungstates, which are the best known wolframites, but also tantalates and niobates, with an isomorphic ambient-pressure wolframite structure, have been included in this review. Apart from estimating the bulk moduli of all known wolframites; the cation-oxygen bond distances and their change with pressure have been correlated with their compressibility. The composition variations of all wolframites have been employed to understand their different structural phase transitions to post-wolframite structures as a response to high pressure. The number of Raman modes and band gap energy changes have been also analyzed in the basis of these compositional differences. The reviewed results are relevant for both fundamental science and for the development of wolframites as scintillating detectors. The possible next research venues of wolframites have also been evaluated.

Keywords: wolframite, high-pressure, phase transitions, crystal structure, phonons, band structure.

I. INTRODUCTION

Wolframite is an iron manganese tungstate mineral. The name is normally used to denote the family of isomorphic compounds. The crystal structure of a wolframite was first solved for $MgWO_4$ by Broch [1] in 1929 with the exception of the oxygen positions and then completely determined for $NiWO_4$ by Keeling [2] in 1957. The structure of wolframite, monoclinic with space group $P2/c$, is adopted by all tungstates AWO_4 with the divalent cation A with an ionic radius in octahedral coordination $r_A < 0.9$ Å. In addition, $CdWO_4$, both M = In and Sc niobates $MNbO_4$ and tantalates $MTaO_4$, and a metastable high-pressure and high-temperature polymorph in molybdates $AMoO_4$ [3] have an analogue crystal structure. Most wolframites, and in particular tungstates and molybdates with an A^{2+} cation with a completely empty or full outer d shell, have been extensively studied for their applications in scintillating detectors for x-ray tomography, high-energy particle physics, and dosimetry devices [4 - 6]. The reason behind this is their high light yield when hit by γ-particles or x-rays despite long scintillation times of a few μs [7]. In fact, the search of different polymorphs of the scintillating wolframites with enhanced properties, i.e. faster scintillating response, has motivated the study of these materials under high pressure conditions. In addition, wolframites with transition metals with unfilled outer d-shells are magnetic. In particular, hübnerite $MnWO_4$, which shows three different antiferromagnetic phases below 13.7 K, is a type II multiferroic material [8, 9], exhibiting ferroelectricity induced by helical magnetic ordering.

After the pioneering work of Young and Schwartz [3], dated from 1963, in which the synthesis of different wolframite-type molybdates was reported at pressures of ~0.6 GPa and 900 ºC, only two works were published about the high-pressure behavior of wolframites during the 1990s. A detailed structural study of the wolframite structure of $MgWO_4$, $MnWO_4$, and $CdWO_4$ was performed at room-temperature by

Macavei and Schultz [10] up to 9.3 GPa using single crystal x-ray diffraction (XRD). A Raman spectroscopy study of $CdWO_4$ up to ~40 GPa was carried out by Jayaraman *et al.* [11] in which a structural phase transition of $CdWO_4$ was found at 20 GPa. However, during the last decade the interest on the behavior under high pressure of wolframites has boosted many works that have contributed to improve the understanding of their structural [12 -16], vibrational [15 - 21], and electronic [14, 22] properties under compression.

In the next sections we shall review first the main features of the behavior and trends of the structure of wolframites under high pressure and the advances on the structural determination of their high-pressure phases. Finally, the effects of pressure on the vibrational, electronic, and optical properties shall be presented with special depth on $CdWO_4$ which high-pressure phase has been recently fully solved.

II. THE WOLFRAMITE STRUCTURE AT HIGH PRESSURE

The best description of the wolframite structure at ambient pressure was formulated by Kihlborg and Gebert [23] in 1969 unfolding the structure of the Jahn-Teller $CuWO_4$ distorted wolframite. The wolframite structure of an AXO_4 compound at ambient conditions [**Fig. 1(a)**] can be described as a framework of oxygen atoms in approximately hexagonal close packing with the cations (*A* and *X*) octahedrally coordinated and occupying half of the octahedral sites. In this structure the octahedral units of the same cations share edges forming alternating zig-zag chains and conferring the structure a layer-like *AOXO* configuration along the [100] direction. A particular case worth of mention is $CuWO_4$, not included in the list of wolframites presented in the introduction. Despite, according to the ionic radius of Cu, it should also crystallize in the same structure as $NiWO_4$ and $ZnWO_4$, it does it in a distorted version of the wolframite structure. In $CuWO_4$, as a consequence of the Jahn-Teller effect of Cu^{2+} in

octahedral coordination [23, 24], the Cu^{2+} ion requires a distortion which is achieved by a shear parallel to the *b* axis along each copper plane. This has as a consequence a displacement of the oxygen layers with each other destroying the twofold symmetry and lowering the space group from $P2/c$ to $P\bar{1}$.

In wolframites the monoclinic *a* and *c* unit-cell lattice parameters are similar although the *c* axis is slightly larger than the *a* axis. However, the *b* axis is, in general, around a 15% larger than the other axes. The monoclinic angles are always very close to 90º. As it was first shown by Macavei and Shultz [10] in $MgWO_4$, $MnWO_4$, and $CdWO_4$, this results in the wolframite structure suffering an anisotropic contraction under pressure (**Fig. 2**). For instance, in $MnWO_4$ [13] the axial compressibility of the *b* axis (k_b = -3.3(1) $\times 10^{-3}$ GPa^{-1}) almost doubles the axis compressibility of *a* and *c* (k_a = -2.0(1) $\times 10^{-3}$ GPa^{-1} and k_b = -1.6 (1) $\times 10^{-3}$ GPa^{-1}). This fact, together with a continuous increase of the monoclinic β angle, indicates that under compression the monoclinic structure tends to distort, at least in tungstates. We shall show in the next section that this continuous distortion conducts to a phase transition to a structure with a lower symmetry in most wolframite-type tungstates. The only exception is $CdWO_4$ that increases its symmetry at the phase transition. In the structure of wolframite the octahedra of different cations only share corners between them, while octahedra of the same cation share both corners and edges. Hence, we can isolate the AO_6 and XO_6 polyhedral units as independent blocks in the structure. In this picture, each type of polyhedra would respond differently to the effect of pressure. In particular, one would expect the XO_6, with high valence (6^+ in W or Mo, and 5^+ in Ta or Nb) to be much less compressible than the *A* cations with 2^+ or 3^+ valences. Such approach has been often used to study the bulk compressibility of scheelites, a structure adopted by tungstates with *A* cations with a large ionic radius. However, differently to wolframites, in

scheelites, the also isolated *X* cations are tetrahedrally coordinated. Therefore, the XO_4 polyhedra are almost pressure independent and the bulk modulus is very well predicted by the empirical equation $B_0 = N \cdot Z/d_{A\text{-}O}^3$, first proposed by Hazen and Finger [25], that considers that the bulk modulus is proportional to the formal charge of the *A* cation, *Z*, and inversally porportional to the cation-anion distance to the third power $d_{A\text{-}O}^3$. In the case of scheelites this proportion constant is N = 610 [26]. The question is how such model would work for wolframites. In **Fig. 3** we show the estimated and experimentally available bulk modulus of all known wolframites. The agreement is excellent considering N = 661 for wolframite-type tungstates and molybdates and N = 610 for tantalates and niobates, indicating that assuming the XO_6 in wolframites as a rigid and almost pressure incompressible unit is also a good assumption in terms of the bulk modulus. In section IV we shall study how this approximation works in terms of describing the grüneissen parameters of the Raman-active modes. The experimental bulk modulus values are shown in **Table I**. **Fig. 3** also shows that the bulk moduli of tantalates and niobates is around 30% larger than for wolframites. This fact, a result of a higher valence of the *A* cation (3+ instead of 2+), reinforces the negligible effect of pressure on the XO_6 polyhedra since the empirical formula is also valid despite the valence of Ta and Nb is 5^+ instead of 6^+.

Regarding the atomic positions under compression in wolframites, while the oxygen atoms barely change their positions, the cations tend to shift along the high symmetry *b* axis [10]; the *A* cations either shift down or up depending on the compound but the W cations largely shift down along the *b* axis. For tantalates and niobates no reliable atomic positions exist under pressure.

III. PHASE TRANSITIONS

Under compression most wolframites undergo a phase transformation to a different polymorph, with tungstates transiting at around 20 GPa and $InTaO_4$ and $ScNbO_4$ doing so a few GPa below. However, the post-wolframite phase depends on the compound. Thus, while tungstates, except $CdWO_4$, apparently transform to a triclinic version of wolframites, similar to that of $CuWO_4$, with space group $P\bar{1}$ and a similar unit-cell; tantalates and niobates also do it but to another distorted version of wolframite that keeps the same space group $P2/c$. $CuWO_4$ and $CdWO_4$ are the only (pseudo)wolframites that under pressure increase their symmetry with $CuWO_4$ transforming to a normal wolframite structure with space group $P2/c$ despite keeping the Jahn-Teller distortion, and $CdWO_4$ introducing a screw axis in space group $P2_1/c$ and doubling the unit cell. The solution of the high-pressure phase of the tungstates has been approached unsuccessfully with powder x-ray diffraction in $ZnWO_4$ and $MgWO_4$ [12] and with single crystal x-ray diffraction in $MnWO_4$ [13]. However, based on the careful indexation of the observed reflections, the study of the systematic extinctions of the high- pressure phase, and the number of active Raman modes observed in the high-pressure phase, that we shall show in the next section, a triclinic structure is proposed as the post-wolframite structure of normal wolframites. This proposed post-wolframite structure would be very similar to the low-pressure phase, but described in space group $P\bar{1}$. Unfortunately, in the particular case of $MnWO_4$, the single crystal, despite of a small volume collapse of only 1% in the phase transition, dramatically deteriorates (**Fig. 4**) with the appearance of more than two triclinic high-pressure domains during the phase transition coexisting with the monoclinic low-pressure phase. This fact prevents a correct integration of the reflections intensities and therefore an accurate determination of the atomic positions in the high-pressure phase.

Preprints (www.preprints.org) | NOT PEER-REVIEWED | Posted: 8 January 2018 doi:10.20944/preprints201801.0070.v1

Peer-reviewed version available at Crystals 2018, 8, 71; doi:10.3390/cryst8020071

In the previous section we have mentioned that $CdWO_4$, with Cd having an ionic radius in octahedral coordination above 0.9 Å, is just above the limit to be a wolframite at ambient pressure. This implies that the Cd-O distances are larger than the *A*-O distances in the remaining wolframites and therefore its bulk modulus is the lowest one in the series (**Fig. 3**). In the extreme case of $MgWO_4$ the Cd-O distances are around 12% longer than the Mg-O distances and the bulk modulus of $MgWO_4$ is 25% larger than that of $CdWO_4$. These differences have an influence in the phase transition of $CdWO_4$ that emerge for instance in the Raman spectrum of the high-pressure phase of $CdWO_4$ presenting 36 instead of the 18 modes observed in the post-wolframite phase of normal wolframites (section IV). In fact, such an increase of modes relates to the doubling of the unit cell that the post-wolframite of $CdWO_4$ presents above 20 GPa. The structure [**Fig. 1 (c)**] was solved with single-crystal x-ray diffraction at 20 GPa [14]. According to Macavei and Shultz [10], the *y* coordinate of Cd moves fast under pressure. In the phase transition, the *a* axis of the high-pressure unit cell remains in the [100] direction of the low-pressure cell increasing its length while the new [010] and [001] directions form from the $[0\bar{1}1]$ and $[0\bar{1}\bar{1}]$ directions of the low-pressure wolframite cell, respectively. Such transformation that can be summarized in the transformation matrix [1 0 0, 0 $\bar{1}$ 1, 0 $\bar{1}$ $\bar{1}$] implies a doubling of the unit cell from $Z = 2$ in the wolframite structure to the $Z = 4$ of the post-wolframite of $CdWO_4$. Such reconstructive phase transition gives rise to the formation of a screw axis along the [010] direction of the high-pressure phase and therefore a symmetry increase from $P2/c$ to $P2_1/c$. Regarding the coordination of the tungsten and cadmium ions, it is increased to [7]-fold and [6+1]-fold, respectively, when the phase transition occurs [**Fig. 1(c)**]. This coordination increase contrasts with the phase transition undergone by normal wolframites which keep the same octahedral coordination for both cations up to the

highest pressure reached according to Raman spectroscopy in the case of the other tungstates. According to powder x-ray diffraction a coordination increase occurs at the phase transition also in tantalates and niobates. Considering that the Cd-O distances are abnormally large in the wolframite-type structure, the coordination increase associated to the phase transition, relates well with $CdWO_4$ which finds a more compact and stable structure that differs more from the wolframite-type structure than the high-pressure phase of the wolframite-type tungstates that keep the cationic coordination. This coordination change is directly related to a band-gap energy drop associated to the phase transition as we shall show in section IV [14].

In the case of $InTaO_4$ and $InNbO_4$ both compounds undergo phase transitions at 13 and 10.8 GPa, respectively. These are pressures around 10 GPa below the phase transition of wolframite-type tungstates. This indicates that when the *X* cation is substituted by Ta or Nb, the wolframite structure becomes less robust, probably, as the result of the lowering of the nominal charge of the ion and therefore weakening the *X*-O bond. Under high pressure, $InTaO_4$ and $InNbO_4$ undergo the same phase transition to a structure [**Fig. 1 (b)**] solved with powder x-ray diffraction [15,16]. Their post-wolframite structure consists on a packing of the wolframite-type structure with the *X* cations increasing their coordination from 6 to 8-fold filling the channels that the alternating *AOXO* zigzag chains create along the [001] direction in the wolframite structure. These alternating pattern is kept in the high-pressure phase but with the *A* and *X* cations having an eight-fold coordination in the high-pressure phase. The coordination increase of both kind of cations and the packing increase generates a different interaction between the AO_8 and XO_8 polyhedra that now share also edges in addition to corners between them. This implies that they cannot longer be considered as separated blocks.

In order to conclude this section, we shall comment on the case of $CuWO_4$ which despite presenting a distorted triclinic version of the monoclinic wolframite structure at ambient pressure, also transforms to the monoclinic wolframite structure above ~9 GPa [23]. As we have explained in the previous section, the low-pressure structure of $CuWO_4$ is also formed by CuO_6 and WO_6 polyhedra arranged in a very similar way to wolframite. However, due to the degeneracy breaking of the $3d^9$ orbitals of Cu^{2+} into five electronic levels (two singlets and one doublet) as the result of the Jahn-Teller effect, two of the six Cu-O distances are longer than the other four, thus, lowering its local structure from quasi O_h to quasi D_{4h} symmetry. Under high-pressure the two longest Cu-O distances reduce but before quenching the Jahn-Teller distortion the system finds an easy distortion direction and the elongated axes of the CuO_6 polyhedra shift from the $[11\bar{1}]$ in the low-pressure phase to the [101] in the high-pressure phase. Thus, the structure transforms to a wolframite structure in space group $P2/c$ that still accommodates the Jahn-Teller distortion of Cu^{2+}.

III. RAMAN SPECTROSCOPY

Raman spectroscopy is a technique used to observe vibrational modes in a solid being one of the most informative probes for studies of material properties under high-pressure [24]. Since the study performed two decades ago by Fomichev *et al.* in $ZnWO_4$ and $CdWO_4$ [25] the Raman spectra of wolframite-type tungstates have been extensively characterized. Studies have been carried out for synthetic crystals [17 – 20] and minerals [26]. They have been also performed in $InTaO_4$ [15] and $InNbO_4$ [16]; however, the characterization of the Raman-active vibrations in wolframite-type molybdates is missing. Indeed, the Raman spectra of $CoMoO_4$, $MnMoO_4$, and $MgMoO_4$ have been characterized [27 - 29], but for polymorphs different than wolframite.

According to group-theory analysis, a crystal structure isomorphic to wolframite has 36 vibrational modes at the Γ point of the Brillouin zone: $\Gamma = 8A_g + 10B_g + 8A_u + 10\ B_u$. Three of these vibrations correspond to acoustic modes ($A_u + 2B_u$) and the rest are optical modes, 18 of which are Raman active ($8A_g + 10B_g$) and 15 of which are infrared active ($7A_u + 8B_u$). Typical Raman spectra, taken from the literature [17 – 20] of wolframite-type tungstates are shown in **Fig. 5**. In the figure, it can be seen that the frequency distribution (and intensity) of the Raman-active modes is qualitatively similar in $CdWO_4$, $ZnWO_4$, $MnWO_4$, and $MgWO_4$. Since Raman-active vibrations correspond either to A_g or B_g modes, polarized Raman scattering and selection rules can be combined to identify the symmetry of modes [30, 31]. The expected eighteen Raman modes have been measured for $CdWO_4$, $ZnWO_4$, $MnWO_4$, and $MgWO_4$ and fifteen modes for $CoWO_4$, $FeWO_4$, and $NiWO_4$. The frequencies of the modes are summarized in **Table II**. As we commented above the frequency distribution of modes is similar in all the tungstates, with four high-frequency modes, two isolated modes around 500 – 550 cm^{-1}, and the remaining twelve modes at frequencies below 450 cm^{-1} in all the compounds.

The similitude among the Raman spectra of wolframite-type tungstates can be explained, as a first approximation, by the fact that Raman modes can be classified as internal and external modes with respect to the WO_6 octahedron [19]. Six internal stretching modes are expected to arise from the WO_6 octahedron. Four of them should have A_g symmetry and the other two B_g symmetry. Since the W atom is heavier than any of the divalent cations in AWO_4 wolframites (e.g. Mg or Mn) and W-O covalent bonds are less compressible than *A*-O bonds, the internal stretching modes of WO_6 are the four modes in the high-frequency part of the Raman spectrum ($2\ A_g + 2\ B_g$) plus one A_g mode located near 550 cm^{-1} and one A_g mode with frequency near 400 cm^{-1}. To

facilitate the identification by the reader the six internal modes are identified by an asterisk in **Table II**. Notice that these six modes have pressure coefficients which do not change much from one compound to the other, and are among the largest pressure coefficients ($d\omega/dP$). These observations are consistent with the fact that these modes are associated to internal vibrations on the WO_6 octahedron and with the well-known incompressibility of it [10], explained in the previous section.

The twelve Raman modes not corresponding to internal stretching vibrations of the WO_6 octahedron imply either bending or motions of WO_6 units against the divalent atom *A*. These modes are in the low-frequency region and are of particular interesting because they are very sensitive to structural symmetry changes. Most of these modes (except to B_g modes) have smaller pressure coefficients than the internal modes. As expected, all Raman-active modes harden under compression, which indicate that the phase transitions induced by pressure are not associated to soft-mode mechanisms. A similar behavior has been reported for wolframite-type $MnWO_4$-$FeWO_4$ solid-solutions [32].

Raman spectroscopy is very sensitive to detect pressure-driven phase transitions in wolframites. In order to illustrate it, we show in **Fig. 6** a selection of Raman spectra measured in $MnWO_4$ at different pressures. The experiments were carried out in a diamond-anvil cell using neon as pressure medium to guarantee quasi-hydrostatic conditions [20]. Clear changes in the Raman spectrum are detected at 25.7 GPa. In particular, new peaks are detected. These changes are indicative of the onset of a structural phase transition. Above 25.7 GPa, gradual changes occur in the Raman spectrum, disappearing the Raman modes of the low-pressure wolframite phase only beyond 35 GPa, which indicate the completion of the phase transition. In parallel the Raman modes of the HP phase steadily gain intensity from 25.7 to 35 GPa. In **Fig. 6**,

the Raman spectra reported at 37.4 and 39.3 GPa correspond to a single post-wolframite phase. The number of Raman-active modes detected for this HP phase of $MnWO_4$ is eighteen (the same number than in the wolframite-type phase). These modes have been assigned in accordance with the crystal structure proposed for the HP phase [13, 31]. This structure is a triclinic distortion of wolframite, and the same number of Raman-active modes are expected; however, all of them have a A_g symmetry in the HP phase. **Table III** gives the frequencies of the Raman-active modes of the HP phase of $MnWO_4$ and its pressure coefficients. A detailed discussion of the Raman spectrum of the HP phase can be found elsewhere [20] and is beyond the scope of this article. Here, we will just mention the most relevant features of it. 1) The modes are not any more isolated in three groups, which suggests that vibrations cannot be explained with the model that considers that the WO_6 octahedron is an isolated unit. 2) The most intense mode is the highest frequency mode (**Fig. 6**), which indicates that it can be associated to a W-O stretching vibration. 3) Interestingly, this mode drops in frequency in comparison to the highest frequency mode in the low-pressure wolframite phase. This is indicative of an increase in W–O bond length evolving towards an effective increasing of the W–O coordination. 4) All the modes of the HP phase harden under compression, but the pressure coefficients of the different modes are smaller than in the low-pressure phase, which can be explained by the decrease of the compressibility of $MnWO_4$.

Phase transitions are detected by Raman spectroscopy in other AWO_4 tungstates from 20 to 30 GPa [17 – 19]. In $CdWO_4$, $ZnWO_4$, and $MgWO_4$ phase coexistence is found between the low- and high-pressure phases in a pressure range of 10 GPa. In all the compounds studied up to now, the Raman spectra of the HP phase resemble very much those of the HP phase of $MnWO_4$. However, there are small discrepancies that suggest that, despite being all the HP phase structurally related to wolframite, there are

some differences in the their HP phases. These can be clearly seen when comparing the Raman spectra published for the HP phases of $CdWO_4$ [18] and $MnWO_4$ [20]. In $CdWO_4$ the phase transition to the post-wolframite structure leads to a doubling of the unit-cell (hence, the formula unit increases from 2 to 4) [14], with the consequent increase in the number of Raman modes. They have been assigned to 19 A_g + 17 B_g modes. Out of them, only twenty-six modes have been observed [14, 18]. The frequency of these modes and the pressure coefficients are summarized in **Table IV**. These values agree very well with theoretical predictions for the monoclinic HP phase of $CdWO_4$ [18]. The larger number of modes observed in the HP phase of $CdWO_4$ in comparison with $MnWO_4$ clearly indicates that the crystal structures of the two compounds are different. In spite of this fact, in the post-wolframite phase of $CdWO_4$, there is a substantial drop of the frequency of the highest frequency mode (the most intense one), as observed in $MnWO_4$ [20]. In the case of $CdWO_4$, a clear correlation can be stablished between the frequency drop of this W-O stretching mode and the increase of the tungsten-oxygen coordination number [13]. Regarding the pressure dependence of the Raman modes in post-wolframite $CdWO_4$, in **Table IV** it can be seen that as in $MnWO_4$, in the HP of $CdWO_4$ phase the vibrational modes are less affected by compression. In the HP phase of $CdWO_4$ there are two modes with negative pressure coefficients. The existence of modes with negative pressure slopes might be an indication of structural instability like that observed in related scheelite-type tungstates [33].

To conclude the discussion on tungstates, we would like to state that in $ZnWO_4$ and $MgWO_4$ [7, 19] less than eighteen Raman modes have been found for the HP phase. The frequency distribution of Raman modes resembles more that of $MnWO_4$ than that of $CdWO_4$. However, no definitive conclusion can be stated on the structure of the HP

phase of $ZnWO_4$ or $MgWO_4$ only from Raman measurements. Indeed, the accurate assignation of the modes of the HP phases of $ZnWO_4$ and $MgWO_4$ is waiting for HP single-crystal experiments similar to those already carried out in $MnWO_4$ and $CdWO_4$ [13, 14].

High-pressure Raman studies have been also carried out for wolframite-type $InTaO_4$ and $InNbO_4$ [15, 16]. In both compounds the Raman spectrum and its pressure evolution resemble that above described for the tunsgtates. Again, in the low-pressure phase, the modes that change more under compression are the highest frequency modes which correspond to internal stretching vibrations of the TaO_6 or NbO_6 octahedron. In these compounds the phase transition occurs around 15 GPa. At the transition there is a redistribution of the high-frequency modes (which seems to be a finger print of the transition to post-wolframite) which involves a drop in frequency in the highest frequency mode and other changes consistent with the coordination changes determined from XRD experiments [15, 16].

IV. ELECTRONIC STRUCTURE AND BAND GAP

The knowledge of the electronic band structure of wolframite-type compounds is important for the developing of technological applications of these materials. The study of the pressure effects in the band gap has been proved to be an efficient tool to test the electronic band structure of materials. The first efforts to accurately determine the band structure of wolframites were made by Abraham *et al.* [34]. These authors focused in $CdWO_4$ comparing it with the better known scheelite-type $CdMoO_4$. By means of density-functional theory calculations, they found that the lower-conduction bands of $CdWO_4$ are controlled by the crystal-field-split of the 5*d* bands of tungsten (slightly hybridized with O 2*p* states). On the other hand, the upper part of the valence band is mainly contributed by O 2*p* states (slightly hybridized with W 5*d* states). As a

consequence, $ZnWO_4$, $CdWO_4$, and $MgWO_4$ have very similar bang-gap energy E_g. Accurate values of E_g have been determined by means of optical-absorption measurements, being E_g equal to 3.98, 4.02, and 4.06 eV in $ZnWO_4$, $CdWO_4$, and $MgWO_4$, respectively [22]. On the contrary, $MnWO_4$ is known to have a considerably smaller band gap, E_g = 2.37 eV [22]. This distinctive behavior is the consequence of the contribution of the Mn $3d^5$ orbitals to the states near the Fermi energy. Basically, Mg ($3s^2$), Zn ($3d^{10}$), or Cd ($4d^{10}$) have filled electronic shells and therefore do not contribute either to the top of the valence band or the bottom of the conduction band. However, in $MnWO_4$, Mn ($3d^5$) contributes to the top of the valence band and the bottom of the conduction band, reducing the band-gap energy in comparison to $ZnWO_4$, $CdWO_4$, and $MgWO_4$. A similar behavior to that of $MnWO_4$ is expected for $NiWO_4$, $CoWO_4$, and $FeWO_4$ due to the presence of Ni $3d^8$, Co $3d^7$, and Fe $3d^6$ states. Therefore, among the wide dispersion of values reported for $NiWO_4$ ($2.28 < E_g < 4.5$) [35], those in the lowest limit appear to be the most realistic values. Notice that the above state conclusions are in agreement with the fact that $CuWO_4$, a distorted-wolframite, in which Cu $3d^9$ states contribute to the top of the conduction band, has a band-gap energy of 2.3 eV [36]. Another relevant difference between the band structure of the first and second group of compounds is that it necessarily implies that $ZnWO_4$, $CdWO_4$, and $MgWO_4$ are direct band gap materials, but the other wolframites are indirect band-gap materials [22].

An analogous behavior to that of the wolframite-tunsgtates is expected for isomorphic molybdates. In this case, the states near the Fermi level will be basically dominated by MoO_4^{2-} [37] and therefore wolframite-type molybdates should have slightly smaller E_g than the tungsten-containing counterpart [38]. Unfortunately, less effort have been dedicated to molybdates than to tungstates. However, the above stated hypothesis has been confirmed in the case of wolframite-type $ZnMoO_4$, which has E_g =

3.22 eV [39]. A similar value is expected for $MgMoO_4$, ruling out estimations that range from 4.5 to 5.5 eV [40]. On the other hand, the band-gap energy of 2.2 eV determined for $NiMoO_4$ [41] is fully consistent with the conclusions extracted from $MnWO_4$. In this case, the Ni $3d^8$ states will be responsible of the reduction of its E_g in comparison with $ZnMoO_4$.

$InTaO_4$ and $InNbO_4$ are promising materials for photocatalytic water splitting applications [42]. Both materials have been found to be indirect band-gap semiconductors, with E_g = 3.79 eV in $InTaO_4$ [16]. In this compound the O 2*p* states, with a small amount of mixing of the In 4*d* states, dominate the upper part of the valence band and Ta 5*d* states and In 5*s* dominate the lower conduction bands. An analogous situation is expected for $InNbO_4$, with the only difference that Nb 4*d* contribute to the bottom of the conduction band and the Ta 5*d* states not. This fact makes E_g slightly smaller in $InNbO_4$ (nearly 3.4 eV) than in $InTaO_4$ [43]. An explanation for this phenomenon comes from the larger Pauling's electronegativity of Nb (1.6) in comparison with Ta (1.5) [44]. Within a basic tight-binding approach, E_g is proportional to the overlap integral between the wave functions of atoms. Since Ta has a smaller Pauling's electronegativity than Nb, in a tantalate, the electron transfer from Ta to neighboring oxygen atoms is expected to be larger than the electron transfer from Nb to the neighboring oxygen atoms in a niobate. Therefore, the superposition of wave functions of Ta and O is larger than that of Nb and O, resulting in a larger E_g in $InTaO_4$ than in $InNbO_4$. The same argument can be used to justify the fact that systematically molybdates have a smaller E_g than tungstates, which has been stated in the previous paragraph.

We shall discuss now the influence of pressure in the band structure of wolframites. We will first focus on wolframite-type tungstates. The pressure

dependence of E_g has been determined from optical-absorption experiments up to 10 GPa for $CdWO_4$, $MgWO_4$, $MnWO_4$, and $ZnWO_4$ [22]. The experiments were carried out on single-crystal samples, under quasi-hydrostatic conditions up to a maximum pressure which is far away from the transition pressure. The obtained results are summarized in **Fig. 7**. There it can be seen that $MnWO_4$ has a very distinctive behavior. For $MgWO_4$, $ZnWO_4$, and $CdWO_4$, the pressure dependence of E_g can be represented by a linear function with a positive slope close to dE_g/dP = 13 meV/GPa [22]. However, a different pressure dependence is followed by $MnWO_4$, in which E_g redshifts at −22 meV/GPa [22]. An explanation to the different behavior of E_g in $MnWO_4$ comes from the contribution of Mn $3d^5$ states to the bottom of the conduction band. Whereas for $MgWO_4$, $ZnWO_4$, and $CdWO_4$, under compression the bottom of the conduction band goes up in energy, the contribution of Mn states makes it to go down [22]. On the other hand, for the four compounds the top of the valence band remains at the same energy. This is translated into an increase of E_g for $MgWO_4$, $ZnWO_4$, and $CdWO_4$, and a decrease of E_g for $MnWO_4$. The same behavior than in $MnWO_4$ has been reported for triclinic wolframite-related $CuWO_4$ [35] and can be predicted for $CoWO_4$, $FeWO_4$, and $NiWO_4$.

The same arguments used to explain the high-pressure behavior of the band-gap in wolframites are useful to understand related scheelite-type and monazite-type oxides [45]. An example of it are scheelite-type $CaMoO_4$ ($CaWO_4$) and $PbMoO_4$ ($PbWO_4$) [46, 47]. Another example of it are monazite-type $SrCrO_4$ and $PbCrO_4$ [48, 49]. In all these compounds the Pb containing compounds have a smaller E_g than their isomorphic compounds. This is due to the contribution of Pb 6*s* (6*p*) states to the top (bottom) of the valence (conduction) band. In addition, the Pb states make the band gap to close under

compression. As a consequence, dE_g/dP is negative in the Pb containing compounds, but has the opposite sign in the other compounds.

Studies beyond the pressure range of stability have been carried out for $CdWO_4$ [14]. In this compound optical-absorption studies under quasi-hydrostatic conditions have been performed up to 23 GPa. The pressure dependence determined of E_g is shown in **Fig. 8**. As described above, in the first compression steps, E_g increases with pressure. However, at 16.9 GPa the behavior of E_g changes, moving to lower energies under compression up to 19.5 GPa. At this pressure a drastic color change occurs in the sample as the result of a sharp band gap reduction to ~3.5 eV [14]. The changes are triggered by the onset of the structural phase transition described in a previous section. In the high-pressure phase of $CdWO_4$ E_g decreases with pressure. Regarding the slope change observed at 16.9 GPa, it is a consequence of a direct to indirect band-gap transition caused by the modification of the electronic band structure under compression [50]. Such band crossing has been also observed in other wolframites, for instance $InTaO_4$ [15]. This phenomenon should influence not only the band gap but also other band-structure parameters, such as the effective masses, having a strong influence in transport properties [51], an issue that deserves to be explored in the future.

Let us discuss now the case of $InTaO_4$. In this compound E_g has been experimentally determined up to 23 GPa [15]. The results are shown in **Fig. 9**. There, it can be seen that when pressure is increased, there is a blueshift of E_g with a dE_g/dP around 5 GPa. As in $CdWO_4$, this singularity occurs due to a band crossing [15], which in the case of $InTaO_4$ is triggered by changes induced in the top of the valence band by pressure. In particular, around 5 GPa the maximum of the valence band change from the Y point of the Brillouin zone to the Z point. On the other hand, when increasing the pressure beyond 13 GPa $InTaO_4$ changes from colorless to yellow [15]. The change in

color is correlated to a band-gap collapse and is associated to a structural phase transition found by Raman and XRD experiments [15]. The HP phase has been found to have a direct band gap (the low-pressure wolframite has an indirect gap). In contrast with the low-pressure phase, in the HP phase E_g redshifts with pressure. This is a consequence of the fact that under compression the valence band shifts slightly faster towards high energies than the conduction band.

To close this section, we would like to comment on the possible pressure-induced metallization of wolframites. It has been suggested, based upon resistivity measurements, that ternary oxides related to wolframite might metallize through band overlaping at relative low pressures (12 – 30 GPa) [52, 53]. So far no evidence of metallization has been detected for all the studied wolframites, either in the pressure range of stability of the low-pressure phase or in the post-wolframite phases up to the maximum pressure achieved in experiments (45 GPa in $ZnWO_4$ and $CdWO_4$) [17, 18]. In particular, the sample darkening associated to a semiconductor–metal transition has never been detected in any wolframite under compression. In addition, density-functional theory calculations also exclude the possibility of metallization in the wolframite and post-wolframite phases [14, 15]. One of the reasons preventing metallization is the robustness of the WO_6 (MO_6, NbO_6, and TaO_6) octahedron which is the less compressible polyhedral unit within the crystal structure. As a consequence, the application of high pressures is not enough to increase the overlap between the electronic wave-functions of transition metals (W, Mo, Nb, and Ta) and oxygen atoms to broaden the electronic bands and create the eventual delocalization of the electrons requested for metallization [54]. The fact that in distorted-wolframite $CuWO_4$ a high-pressure phase transition takes place without any significant reduction of the Jahn-Teller

distortion [55] suggests that this compound is the best candidate for metallization driven by band overlap under compression.

V. CONCLUDING REMARKS

In the sections presented above we have described the recent advances made on the understanding of the structural, vibrational and electronic properties of wolframites under compression. Between those advances, probably the one that has had more influence in the field has been the structural solution of the different post-wolframite structures. The precise knowledge of the pressure structural stability of different wolframites and their high-pressure structures has opened two new venues to explore: i) the study of the scintillating properties of the high-pressure polymorphs by means of high-pressure photoluminescence studies, ii) the changes produced by this structural change on the magnetic properties of those wolframites with an open *d* outer shell like multiferroic $MnWO_4$, and iii) the behavior under compression of wolframite alloys like $MnW_{1-x}Mo_xO_4$ [56]; in particular, $CdW_{1-x}Mo_xO_4$ whose end-members have either the wolframite or scheelite structure. For these biphasic alloy systems their HP behavior is unpredictable [57].

In recent years some works have appeared dealing with the pressure-temperature magnetic phase diagram of pure [58] or cobalt alloyed [59] $MnWO_4$. Those works have found that pressure is able to disrupt the fine equilibrium of the frustrated antiferromagnetic phase of $MnWO_4$ (AF1) but enhance the Néel temperature of the AF3 and AF4 magnetic phases of pure or lowly Co-doped $MnWO_4$ and highly Co-doped $MnWO_4$, respectively. Considering the direct effect that pressure has on the spin structure being even able to cause a spin-flop transition for highly Co-doped $MnWO_4$ [59] one can expect a new and fascinating phase diagram in the high-pressure phase of $MnWO_4$ where distortions are expected to be higher due to the lowering of symmetry

from space group $P2/c$ to $P\bar{1}$. So far, the only study done in this direction has been done with $CuWO_4$ in which according to calculations the structural phase transition from $P2/c$ to $P\bar{1}$ also involves an antiferromagnetic to ferromagnetic order [60].

In summary, despite some fundamental questions still remain to be completely solved, like the crystallization of $CdWO_4$ in a wolframite structure despite of the size of Cd or the atomic coordinates of the post-wolframite phase of $MnWO_4$, this brief review shows: i) the great advance that has been done in this family of compounds since the pioneering works of Macavei and Shultz [10] and Jayaraman et al. [11] and ii) the venues that remain open to be explored.

Acknowledgments

J. Ruiz-Fuertes thanks the Spanish Ministerio de Economía y Competitividad (MINECO) for the support through the Juan de la Cierva Program (IJCI-2014-20513). This work was supported by the Spanish MINECO, the Spanish Research Agency (AEI), and the European Fund for Regional Development (FEDER) under project number MAT2016-75586-C4-1-P. The authors are grateful to all the collaborators who participate in their research on the reviewed subject.

References

[1] E. K. Broch, Skr. Norske Vidensk Akad. Mat. Nat. Klasse **8**, 20 (1929).

[2] R. O. Keeling Jr, Acta Cryst. **10**, 209 (1957).

[3] A. P. Young and C. M. Schwartz, Science **141**, 348 (1963).

[4] S. Rathee, D. Tu, T. T. Monajemi, D. W. Rickey, and B. G. Fallone, Med. Phys. **33**, 1078 (2006).

[5] V. B. Mikhailik and H. Kraus, Phys. Status Solidi B **247**, 1583 (2010).

[6] M. M. Silva, S. M. V. Novais, E. S. S. Silva, T. Schimitberger, Z. S. Macedo, and R. F. Bianchi, Mater. Chem. Phys. **136**, 317 (2012).

[7] S. P. Burachas, F. A. Danevich, A. S. Georgadze, H. V. Klapdor-Kleingrothaus, V. V. Kobychev, B. N. Kropivyansky, V. N. Kuts, A. Muller, V. V. Muzalevsky, A. S. Nikolaiko et al., Nucl. Instrum. Methods Phys. Res., Sect. A **369**, 164 (1996).

[8] G. Lautenschläger, H. Weitzel, T. Vogt, R. Hock, A. Böhm, M. Bonnet, and H. Fuess, Phys. Rev. B **48**, 6087 (1993).

[9] R. P. Chaudhury, F. Yen, C. R. de la Cruz, B. Lorenz, Y. Q. Wang, Y. Y. Sun, and C. W. Chu, Physica B **403**, 1428 (2008).

[10] J. Macavei and H. Schulz, Z. Kristallogr. **207**, 193 (1993).

[11] A. Jayaraman, S. Y. Wang, and S. K. Sharma, Curr. Sci. **69**, 44 (1995).

[12] J. Ruiz-Fuertes, S. López-Moreno, D. Errandonea, J. Pellicer-Porres, R. Lacomba-Perales, A. Segura, P. Rodríguez-Hernández, A. Muñoz, A. H. Romero, and J. González, J. Appl. Phys. **107**, 083506 (2010).

[13] J. Ruiz-Fuertes, A. Friedrich, O. Gomis, D. Errandonea, W. Morgenroth, J. A. Sans, and D. Santamaría-Pérez, Phys. Rev. B **91**, 104109 (2015).

[14] J. Ruiz-Fuertes, A. Friedrich, D. Errandonea, A. Segura, W. Morgenroth, P. Rodríguez-Hernández, A. Muñoz, and Y. Meng, Phys. Rev. B **95**, 174105 (2017).

[15] D. Errandonea, C. Popescu, A. B. Garg, P. Botella, D. Martínez-García, J. Pellicer-Porres, P. Rodríguez-Hernández, A. Muñoz, V. Cuenca-Gotor, and J. A. Sans, Phys. Rev. B **93**, 035204 (2016).

[16] A. B. Garg, D. Errandonea, C. Popescu, D. Martínez-García, J. Pellicer-Porres, P. Rodríguez-Hernández, A. Muñoz, P. Botella, V. P. Cuenca-Gotor, and J. A. Sans, Inorg. Chem. **56**, 5420 (2017).

[17] D. Errandonea, F. J. Manjón, N. Garro, P. Rodríguez-Hernández, S. Radescu, A. Mujica, A. Muñoz, and C. Y. Tu, Phys. Rev. B **78**, 054116 (2008).

[18] R. Lacomba-Perales, D. Errandonea, D. Martínez-García, P. Rodríguez-Hernández, S. Radescu, A. Mújica, A. Muñoz, J. C. Chervin, and A. Polian, Phys. Rev. B **79**, 094105 (2009).

[19] J. Ruiz-Fuertes, D. Errandonea, S. López-Solano, J. González, O. Gomis, R. Vilaplana, F. J. Manjón, A. Muñoz, P. Rodríguez-Hernández, A. Friedrich, I. A. Tupitsyna, and L. L. Nagornaya, Phys. Rev. B **83**, 214112 (2011).

[20] J. Ruiz-Fuertes, O. Gomis, D. Errandonea, A. Friedrich, and F. J. Manjón, J. Appl. Phys. **115**, 043510 (2014).

[21] R. C. Dai, X. Ding, Z. P. Wang, and Z. M. Zhang, Chem. Phys. Lett. **586**, 76 (2013).

[22] J. Ruiz-Fuertes, S. López-Moreno, J. López-Solano, D. Errandonea, A. Segura, R. Lacomba-Perales, A. Muñoz, S. Radescu, P. Rodríguez-Hernández, M. Gospodinov, L. L. Magornaya, and C. Y. Tu, Phys. Rev. B **86**, 125202 (2012).

[23] J. Ruiz-Fuertes, A. Friedrich, J. Pellicer-Porres, D. Erradonea, A. Segura, E. Haussühl, C.-Y. Tu, and A. Polian, Chem. Mater. **23**, 4220 (2011).

[24] A. Goncharov, International Journal of Spectroscopy **2012**, 617528 (2012).

[25] V. V. Fomichev and O. I. Kondratov, Spectrochimica Acta A **50**, 1113 (1994).

[26] M. Crane, R. L. Frost, P. A. Williams, and J. T. Kloprogge, J. Raman Spectrosc. **33**, 62 (2002).

[27] I. Kanesake, H. Hashiba, and I. Matsumura, J. Raman Spectrosc. **19**, 213 (1988).

[28] M. N. Coelho, P. T. C. Freire, M. Maczka, C. Luz-Lima, G.D. Saraiva, W. Paraguassu, A.G. Souza Filho, and P.S. Pizani, Vibrat. Spectrosc. **68**, 34 (2013).

[29] A. P. de Moura, L. H. de Oliveira, P. F. S. Pereira, I. L. V. Rosa, M. S. Li, E. Longo, and J. A. Varela, Advances in Chemical Engineering and Science **2**, 465 (2012).

[30] M. N. Iliev, M. M. Gospodinov, and A. P. Litvinchuk, Phys. Rev. B **80**, 212302 (2009).

[31] D. Errandonea, J. Pellicer-Porres, D. Martínez-García, J. Ruiz-Fuertes, A. Friedrich, W. Morgenroth, C. Popescu, P. Rodríguez-Hernández, A. Muñoz, and M. Bettinelli, J. Phys. Chem. C **120**, 13749 (2016).

[32] M. Maczka, M. Ptak, K. Pereira da Silva, P. T. C. Freire, and J, Hanuza, J. Phys. Condensed Matter **24**, 345403 (2012).

[33] D. Errandonea and F. J. Manjon, Materials Research Bulletin **44**, 807 (2009).

[34] Y. Abraham, N. A. W. Holzwarth, and R. T. Williams, Phys. Rev. B **62**, 1733 (2000).

[35] S. M. M. Zawawi, R. Yahya, A. Hassan, H. N. M. E. Mahmud, and M. N. Daud, Chem. Central Journal **7**, 80 (2013).

[36] J. Ruiz-Fuertes, D. Errandonea, A. Segura, F.J. Manjón, Zh. Zhu, and C.Y. Tu, High Pres. Res. **28**, 565 (2008).

[37] D. Errandonea, Materials Letters **63**, 160 (2009).

[38] R. Lacomba-Perales, J. Ruiz-Fuertes, D. Errandonea, D. Martınez-Garcıa and A. Segura, EPL **83**, 37002 (2008).

[39] L. S. Cavalcante, E. Moraes, M. A. P. Almeida, C. J. Dalmaschio, N. C. Batista, J. A. Varela, E. Longo, M. Siu Li, J. Andrés, and A. Beltrán, Polyhedron **54**, 13 (2013).

[40] D. A. Spasskii, V. N. Kolobanov, V. V. Mikhailin, L. Yu. Berezovskaya, L. I. Ivleva, and I. S. Voronina, Optics and Spectroscopy **106**, 556 (2009).

[41] A. P. de Moura, L. H. de Oliveira, I. L. V. Rosa, C. S. Xavier, P. N. Lisboa-Filho, M. S. Li, F. A. La Porta, E. Longo, and J. A. Varela, Scientific World Journal **2015**, 315084 (2015).

[42] Z. Zou, J. Ye, K. Sayana, and H. Arakawa, Nature **414**, 625 (2001).

[43] G. L. Li and Z. Yin, Phys. Chem. Chem. Phys. **13**, 2824 (2011).

[44] L. Pauling J. Amer. Chem. Soc. **54**, 3570 (1932).

[45] D. Errandonea, Phys. Stat. Sol. B **254**, 1700016 (2017).

[46] V. Panchal, N. Garg, H. K. Poswal, D. Errandonea, P. Rodríguez-Hernández, A. Muñoz, and E. Cavalli, Phys. Rev. Materials **1**, 043605 (2017).

[47] R. Lacomba-Perales, D. Errandonea, A. Segura, J. Ruiz-Fuertes, P. Rodríguez-Hernández, S. Radescu, J. Lopez-Solano, A. Mujica, and A. Muñoz, J. Appl. Phys. **110**, 043703 (2011).

[48] E. Bandiello, D. Errandonea, D. Martinez-Garcia, D. Santamaria-Perez, and F. J. Manjón, Phys. Rev. B **85**, 024108 (2012).

[49] J. Gleissner, D. Errandonea, A. Segura, J. Pellicer-Porres, M. A. Hakeem, J. E. Proctor, S. V. Raju, R. S. Kumar, P. Rodríguez-Hernández, A. Muñoz, S. Lopez-Moreno, and M. Bettinelli, Phys. Rev. B **94**, 134108 (2016).

[50] M. Baj, L. H. Dmowski, and T. Slupinski, Phys. Rev. Lett. **71**, 3529 (1993).

[51] D. Errandonea, A. Segura, F. J. Manjon, and A Chevy, Semicond. Sci. Technol. **18**, 241 (2003).

[52] A.B. Garg, K.V. Shanavas, B.N. Wani, S.M. Sharma, J. Solid State Chem. **203**, 273 (2013).

[53] S. J. Duclos, A. Jayaraman, G. P. Espinosa, A. S. Oxper, and R. G. Maines, J. Phys. Chem. Solids **8**, 769 (1989).

[54] J. R. Patterson, C. M. Aracne, D. D. Jackson, V. Malba, and S. T. Weir, Phys. Rev. B **69**, 220101(R) (2004).

[55] J. Ruiz-Fuertes, A. Segura, F. Rodríguez, D. Errandonea, and M. N. Sanz-Ortiz, Phys. Rev. Lett. **108**, 166402 (2012).

[56] V. Blanco-Gutierrez, A. Demourgues, E. Lebreau, and M. Gaudon, Phys. Stat. Sol. B **253**, 2043 (2016).

[57] A. Taoufyq, F. Guinneton, J. C. Valmalette, M. Arab, A. Benlhachemi, B. Bakiz, S. Villain, A. Lyoussi, G. Nolibe, and J. R. Gavarri, J. Sol. Stat. Chem. **219**, 127 (2014).

[58] R. P. Chaudhury, F. Yen, C. R. de la Cruz, B. Lorenz, Y. Q. Wang, Y. Y. Sun, and C. W. Chu, Physica B **403**, 1428 (2008).

[59] J. Wang, F. Ye, S. Chi, J. A. Fernandez-Baca, H. Cao, W. Tian, M. Gooch, N. Poudel, Y. Wang, B. Lorenz, and C. W. Chu, Phys. Rev. B **93**, 155164 (2016).

[60] J. Ruiz-Fuertes, D. Errandonea, R. Lacomba-Perales, A. Segura, J. González, F. Rodríguez, F. J. Manjón, S. Ray, P. Rodríguez-Hernández, A. Muñoz, Zh. Zhu, and C. Y. Tu, Phys. Rev. B, **81**, 224115 (2010).

Figure Captions

Figure 1. (a) General ambient-pressure wolframite-type structure of ABO_4 and high-pressure structure of (b) $InTaO_4$ and (c) $CdWO_4$.

Figure 2. Pressure dependence of the unit-cell lattice parameters of $MnWO_4$. Empty circles represent Macavei and Schulz data, full circles and triangles show data obatined by powder x-ray diffraction, and the crosses are data obtained by single crystal x-ray diffraction. The continuous lines are fits to a third order Birch Mucrnaghan equation of state.

Figure 3. Volume change of the bulk modulus B_0 of all known compounds with a wolframite-type structure. Circles represent experimental results. Squares are the estimated B_0 considering the WO_6, TaO_6, and NbO_6 as rigid units and the following dependence with the A-O distances: $B_0 = 610*Z/d_{A\text{-}O}^3$ in the case of tantalates and noibates and $B_0 = 661*Z/d_{A\text{-}O}^3$ in the case of wolframites and molybdates.

Figure 4. Section of one single-crystal x-ray diffraction frame of $MnWO_4$ (left) showing the exitence of the reflections of two high-pressure triclinic domains (T1, T2) along the monoclinic (M) one. The corresponding projection of the reciprocal space on the (b^*; c^*) plane (right). Dots represent the location of the measured reflections projected along the a^* axis. The axes of the unit cells are shown as dashed lines. The monoclinic reflections are in black while the triclinic reflections of the two domains are in blue (T1) and red (T2).

Figure 5. Raman spectra of $CdWO_4$, $ZnWO_4$, $MnWO_4$, and $MgWO_4$ at ambient conditions.

Figure 6. Raman spectra of $MnWO_4$ at selected pressures. Raman modes of the wolframite phase are indentified by ticks (an labeled) in the lowest trace (3.6 GPa). At 25.7 GPa the modes of the low- and high-pressure phase are identified by red and gree ticks, respectively. At 37.4 GPa the ticks identify the eighteen Raman-active modes of the HP phase. Pressure (in GPa) are indicated in each Raman spectrum.

Figure 7. Pressure dependence of the band-gap energy in (a) wolframite-type $MgWO_4$, $ZnWO_4$, $CdWO_4$, and (b) $MnWO_4$.

Figure 8. Pressure dependence of the band-gap enery for the low- and high-pressure phases of $CdWO_4$.

Figure 9. (left) Pressure dependence of E_g in the low-pressue phase of $InTaO_4$. The change in the pressure dependence caused by the band-crossing induced by pressure is indicated with arrows. (right) Pressure dependence of E_g in the low- and high-pressue phases of $InTaO_4$. The band-gap collapse associated to the transition is indicated (ΔE_g = 1.3 eV). In both figures symbols correspond to experiments and lines to calculations.

Table I. Experimental bulk modulus (B_0) of different wolframites. Results were obtained from Refs. [10] and [12-16].

compounds	B_0 (GPa)
$MgWO_4$	144 - 160
$MnWO_4$	131 - 145
$ZnWO_4$	145
$CdWO_4$	136 - 123
$InTaO_4$	179
$InNbO_4$	179

Preprints (www.preprints.org) | NOT PEER-REVIEWED | Posted: 8 January 2018 doi:10.20944/preprints201801.0070.v1

Peer-reviewed version available at Crystals 2018, 8, 71; doi:10.3390/cryst8020071

Table II: Raman frequencies, ω (cm^{-1}), measured in different wolframite-type tungstates [17 – 20]. The symmetry of the different modes is given. The pressure coefficients, dω/dP (cm^{-1}/GPa), are included in parenthesis for those compounds that are available. The asterisks identify the internal modes of the WO_6 octahedron.

Mode	$MgWO_4$ ω (dω/dP)	$MnWO_4$ ω (dω/dP)	$ZnWO_4$ ω (dω/dP)	$CdWO_4$ ω (dω/dP)	$FeWO_4$ ω	$CoWO_4$ ω	$NiWO_4$ ω
B_g	97.4 (0.69)	89 (0.73)	91.5 (0.95)	78 (0.52)	86	88	91
A_g	155.9 (0.26)	129 (0.02)	123.1 (0.65)	100 (0.69)	124	125	141
B_g	185.1 (0.51)	160 (0.22)	145.8 (1.20)	118 (1.02)	154	154	165
B_g	215.0 (0.63)	166 (0.78)	164.1 (0.72)	134 (0.82)	174	182	190
B_g	266.7 (1.01)	177 (1.03)	189.6 (0.67)	148 (1.51)		199	201
A_g	277.1 (0.55)	206 (2.01)	196.1 (2.25)	177 (0.71)	208		
B_g	313.9 (1.99)	272 (2.03)	267.1 (1.32)	249 (2.14)	266	271	298
A_g	294.1 (1.92)	258 (0.30)	276.1 (0.87)	229 (0.29)			298
B_g	384.8 (4.95)	294 (2.02)	313.1 (1.74)	269 (1.41)	299	315	
A_g	351.9 (3.52)	327 (1.50)	342.1 (1.74)	306 (0.04)	330	332	354
B_g	405.2 (1.47)	356 (4.09)	354.1 (3.87)	352 (4.55)			
A_{g*}	420.4 (1.59)	397 (1.69)	407 (1.65)	388 (2.33)	401	403	412
B_g	518.1 (3.30)	512 (2.86)	514.5 (3.18)	514 (3.86)	500	496	505
A_{g*}	551.6 (3.00)	545 (2.39)	545.5 (3.00)	546 (2.32)	534	530	537
B_{g*}	683.9 (4.09)	674 (4.20)	677.8 (3.90)	688 (4.35)	653	657	663
A_{g*}	713.2 (3.35)	698 (3.08)	708.9 (3.30)	707 (3.92)	692	686	688
B_{g*}	808.5 (3.69)	774 (3.58)	786.1 (4.40)	771 (4.30)	777	765	765
A_{g*}	916.8 (3.19)	885 (1.63)	906.9 (3.70)	897 (3.66)	878	881	887

Table III: The Raman active modes of the HP phase of $MnWO_4$ at 34 GPa with their pressure coefficients.

Mode	ω (cm^{-1})	dω/dP (cm^{-1} GPa^{-1})
A_g	146	0.8
A_g	186	0.09
A_g	196	1.78
A_g	217	1.73
A_g	242	1.58
A_g	292	0.78
A_g	314	1.34
A_g	370	2.02
A_g	388	2.6
A_g	446	2.46
A_g	495	1.5
A_g	511	1.34
A_g	586	1.19
A_g	676	1.86
A_g	710	1.46
A_g	784	1
A_g	810	3.26
A_g	871	0.69

Table IV: The Raman-active modes of the HP phase of $CdWO_4$ at 26.9 GPa with their pressure coefficients. Twenty-six out of the thirty-six modes expected have been meaured.

Mode	ω (cm^{-1})	dω/dP (cm^{-1} GPa^{-1})
A_g	69	1.96
B_g	88	1.94
A_g	99	0.09
B_g	130	0.38
A_g	146	1.35
A_g	155	0.97
B_g	165	0.19
A_g	185	1.26
B_g	209	1.26
A_g	243	-0.06
B_g	279	2.53
A_g	290	0.99
B_g	315	3.00
B_g	378	1.65
A_g	401	2.31
A_g	428	3.03
B_g	475	2.51
A_g	486	2.71
B_g	512	2.33
B_g	590	2.62
A_g	673	-0.82
A_g	688	2.81
B_g	710	1.60
A_g	766	2.12
A_g	824	2.23
A_g	864	2.04

Figure 1

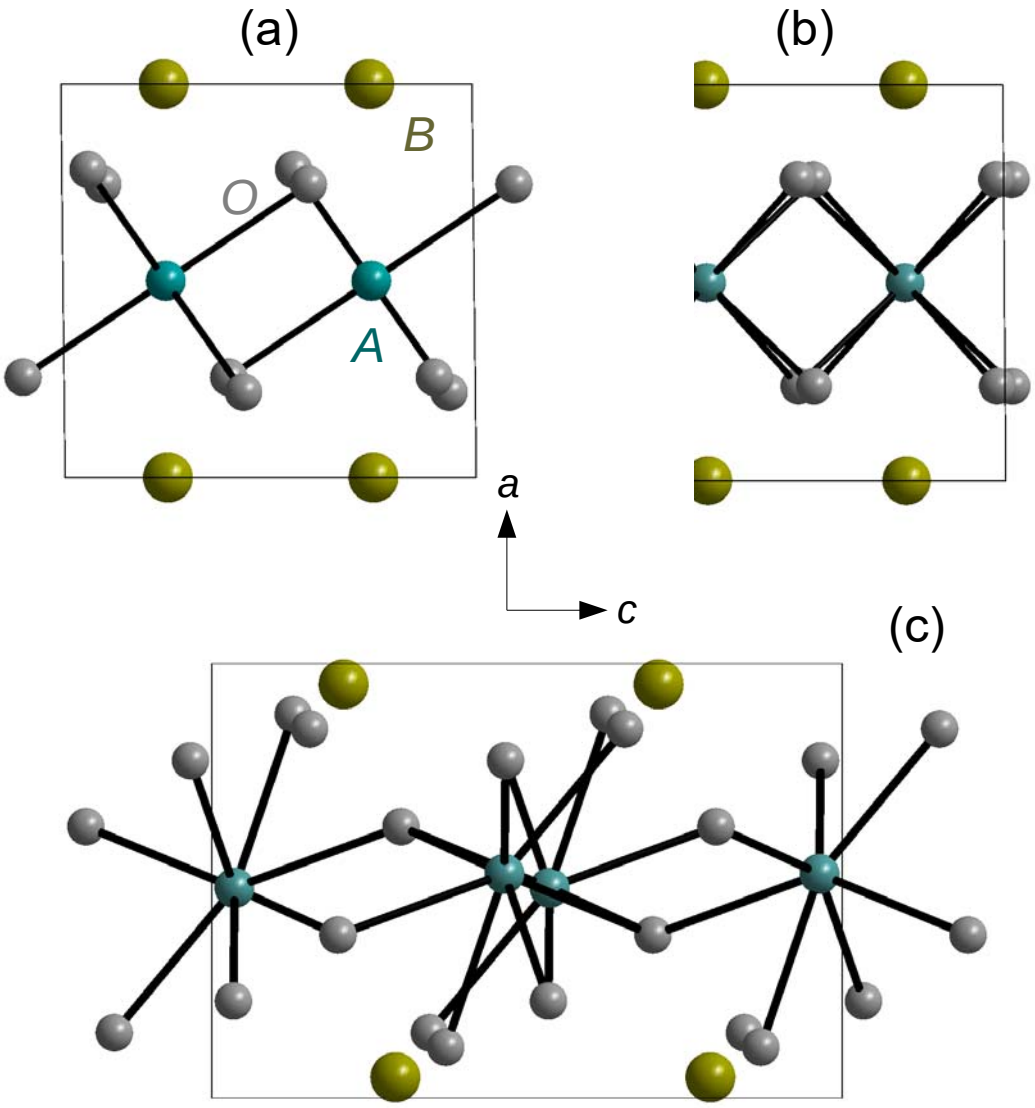

Figure 2

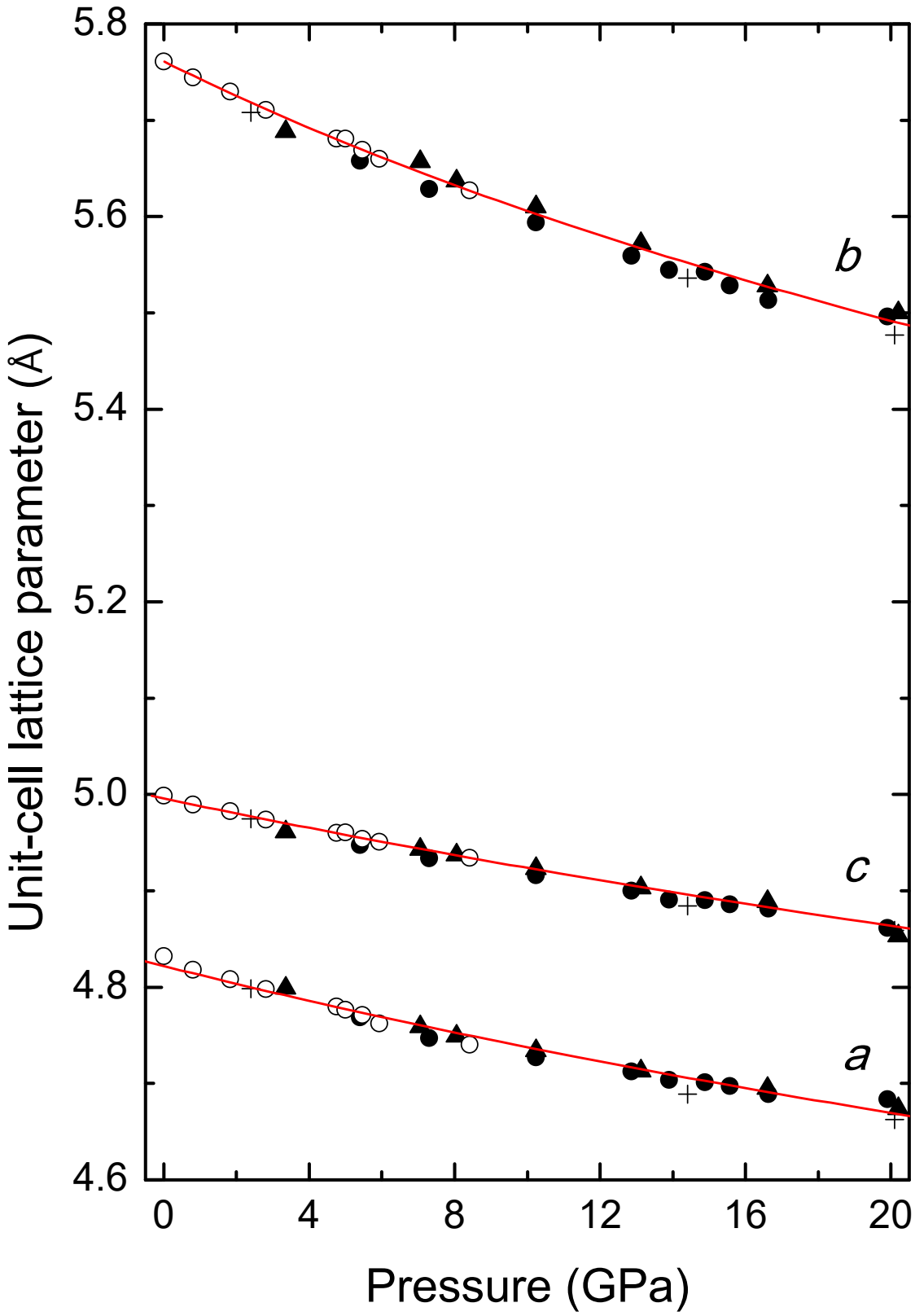

Preprints (www.preprints.org) | NOT PEER-REVIEWED | Posted: 8 January 2018 doi:10.20944/preprints201801.0070.v1

Peer-reviewed version available at Crystals 2018, 8, 71; doi:10.3390/cryst8020071

Figure 3

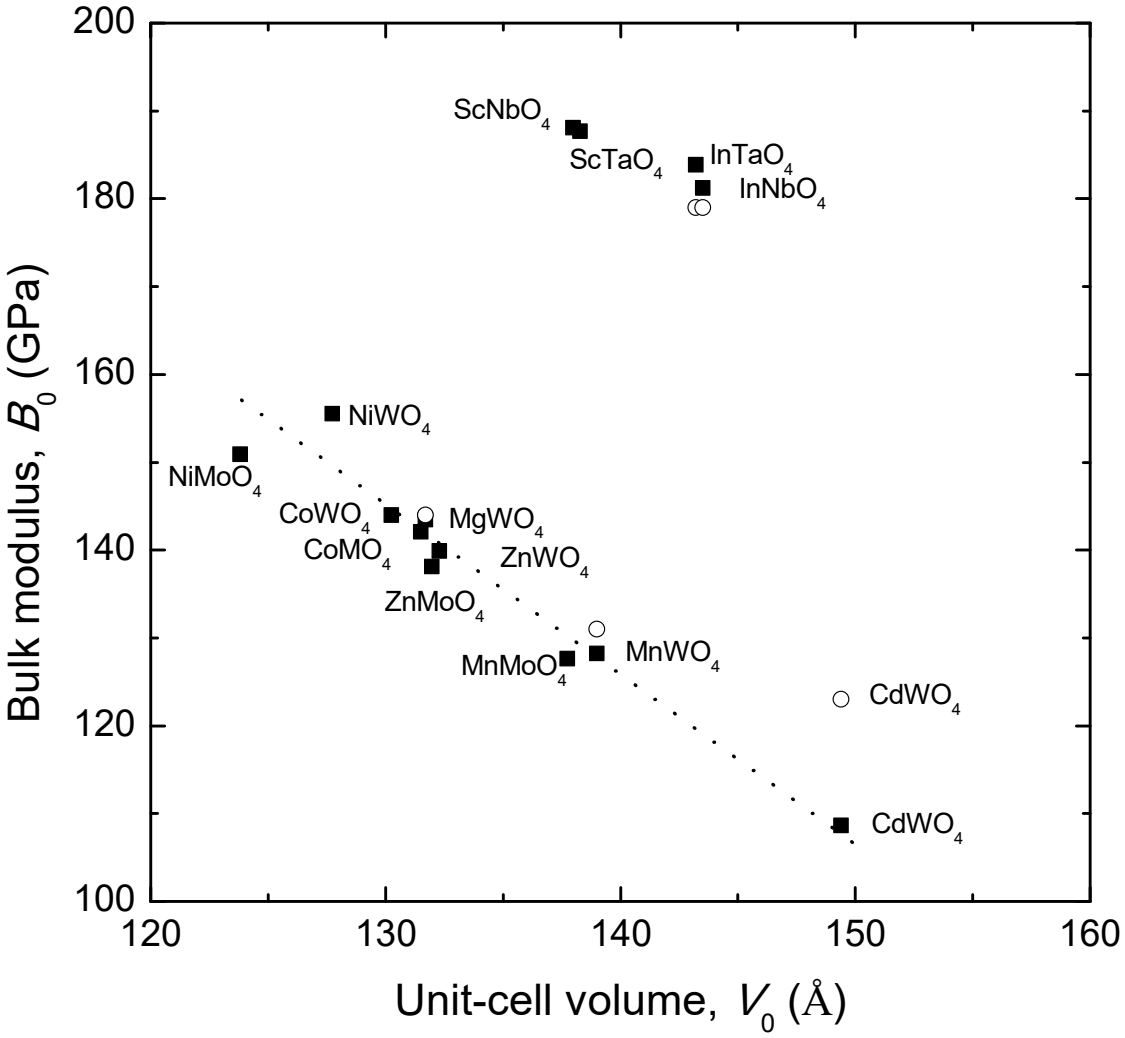

Figure 4

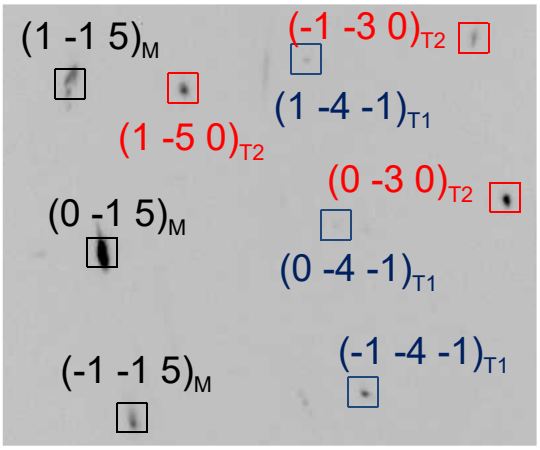

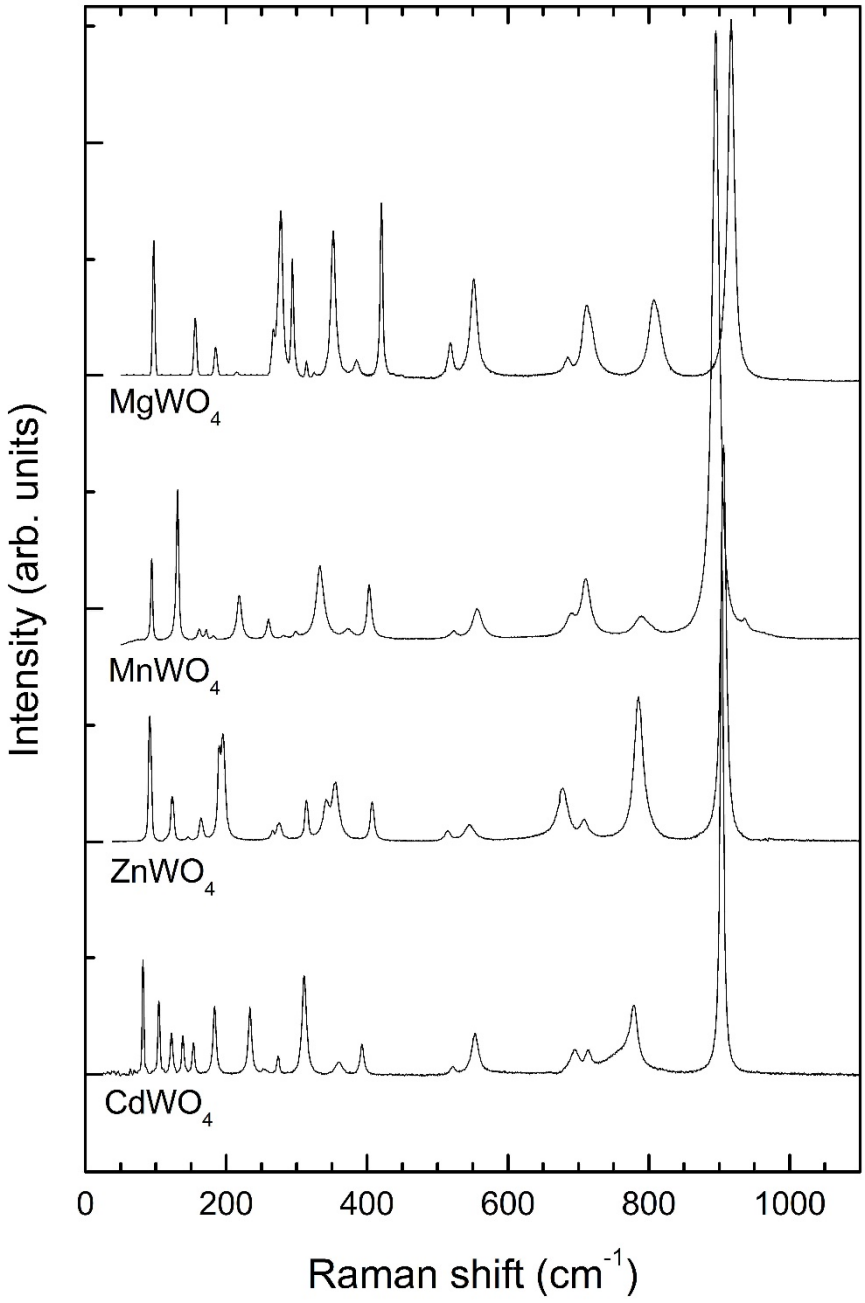

Figure 5

Figure 6

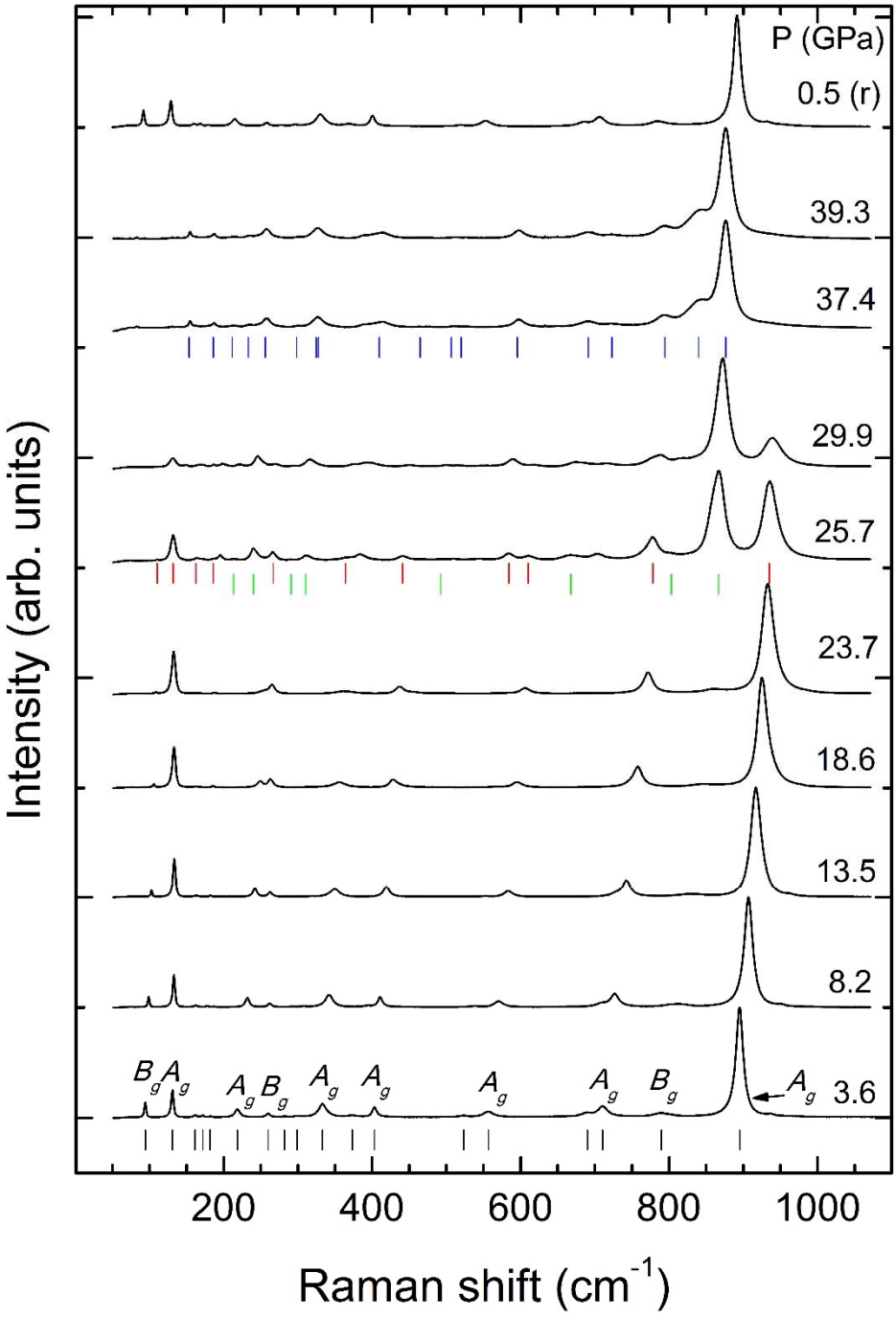

Preprints (www.preprints.org) | NOT PEER-REVIEWED | Posted: 8 January 2018 doi:10.20944/preprints201801.0070.v1

Peer-reviewed version available at Crystals 2018, 8, 71; doi:10.3390/cryst8020071

Figure 7

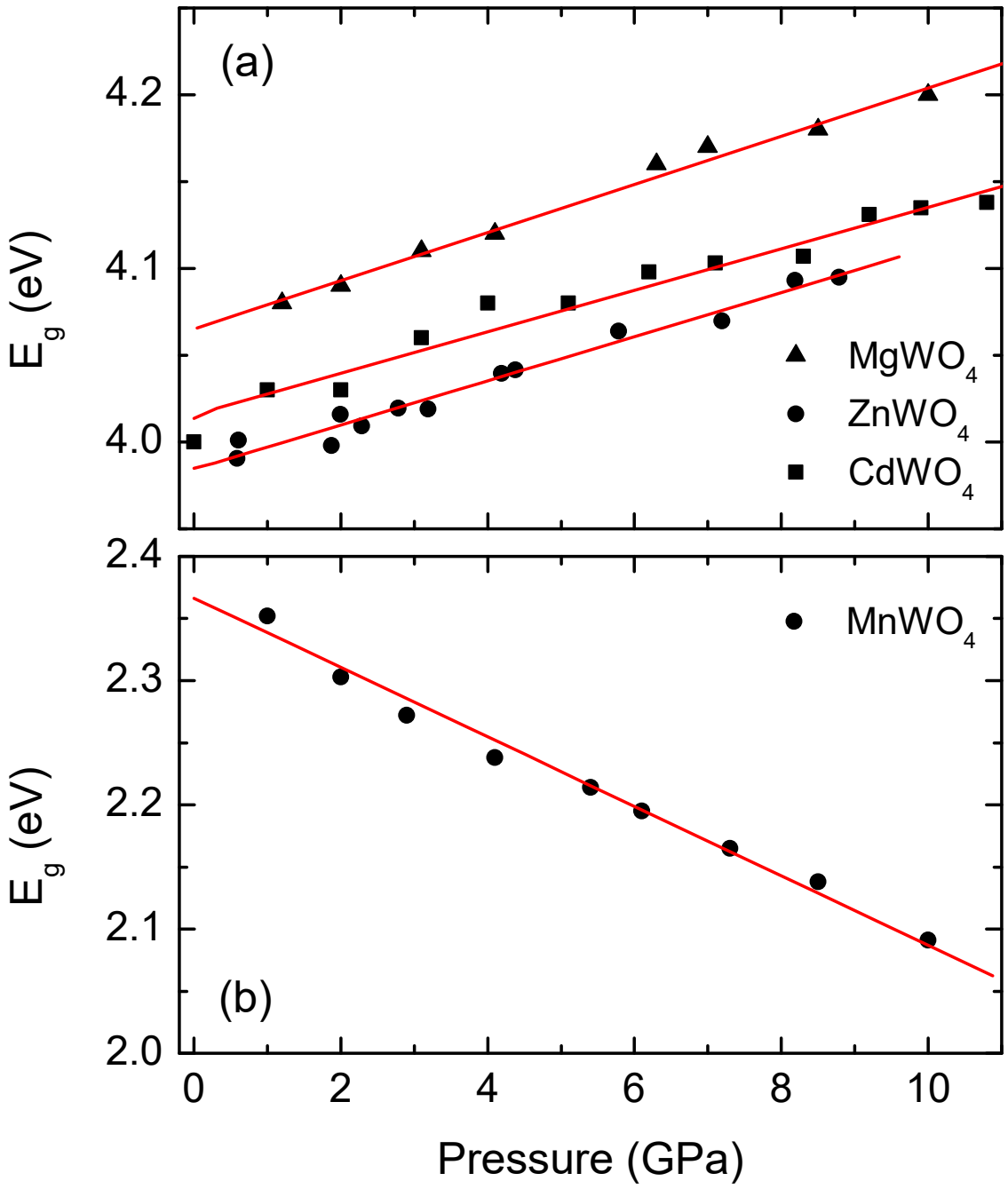

Preprints (www.preprints.org) | NOT PEER-REVIEWED | Posted: 8 January 2018 doi:10.20944/preprints201801.0070.v1

Peer-reviewed version available at Crystals 2018, 8, 71; doi:10.3390/cryst8020071

Figure 8

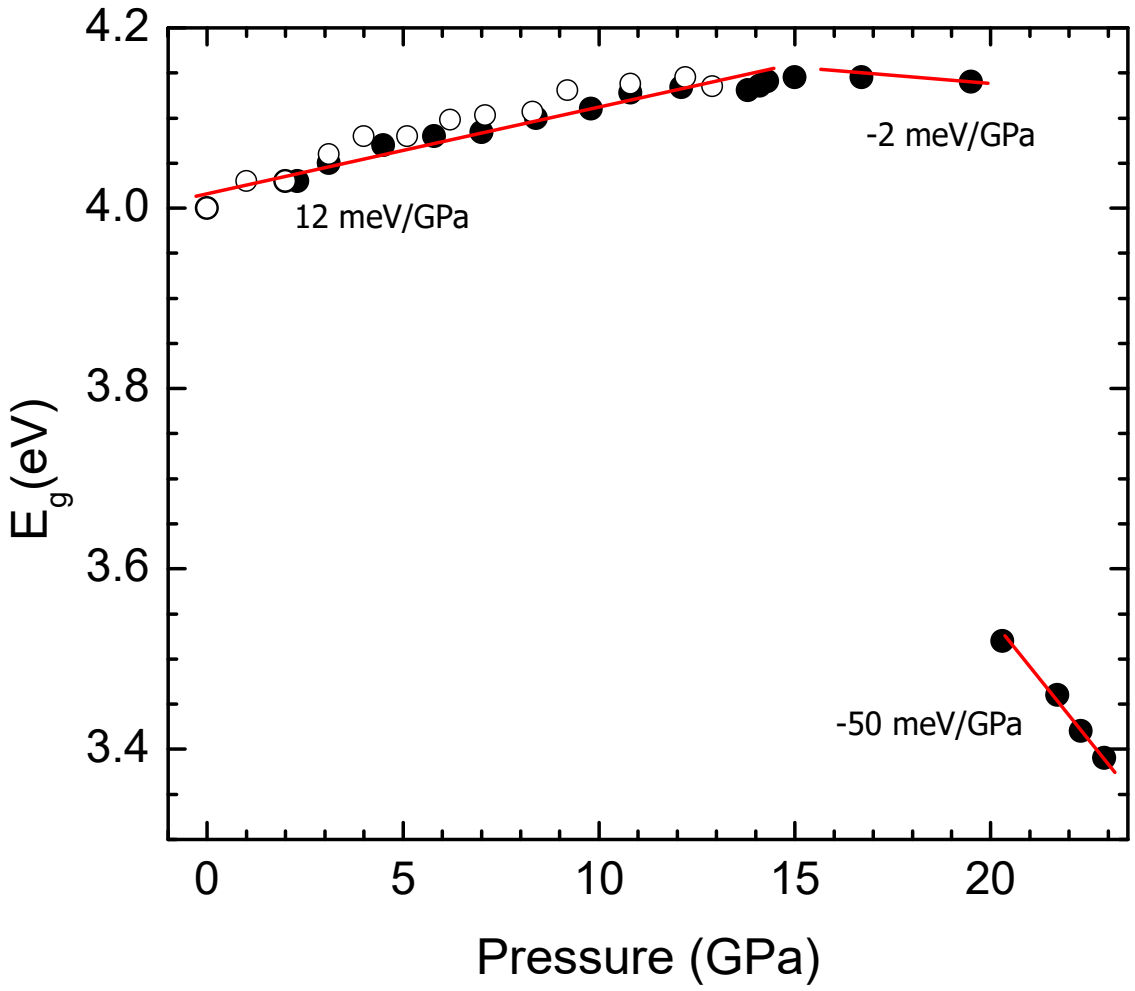

Figure 9